Physica Scripta

INCLUSIVE PUBLISHING TRUSTED SCIENCE

PURPOSE-LED PUBLISHING™

PAPER

A chameleon system with a cosine function: bifurcation analysis, multistability, and offset boosting

To cite this article: Jie Liu *et al* 2025 *Phys. Scr.* **100** 035229

View the article online for updates and enhancements.

You may also like

- A wideband high gain conformal self-decoupled multiport antenna for 5G millimeter wave communications
Priyanka Das and Surajit Kundu
- Dynamic analysis of Hopfield neural network with Sigmoid-type activation function
Yunzhen Zhang, Xiaowei Yin, Chengjie Chen et al.
- Surface modification in $FAPbI_3$ perovskites using methyl-substituted benzene derivatives: impact of functional groups and methyl position
Muhammad Tahir, XiangXiang Feng, Yunhao Li et al.

This content was downloaded from IP address 124.131.235.146 on 24/02/2025 at 15:12

Physica Scripta

PAPER

A chameleon system with a cosine function: bifurcation analysis, multistability, and offset boosting

RECEIVED
25 September 2024

REVISED
21 January 2025

ACCEPTED FOR PUBLICATION
6 February 2025

PUBLISHED
19 February 2025

Jie Liu[1], **Bo Sang**[1], **Chun Wang**[1], **Lihua Fan**[1], **Xueqing Liu**[1], **Irfan Ahmad**[2], **Timur Karimov**[3], **Vyacheslav Rybin**[3], **Denis Butusov**[3] and **Ning Wang**[4]

[1] School of Mathematical Sciences, Liaocheng University, Liaocheng 252059, People's Republic of China
[2] Faculty of Science and Engineering, Maynooth International Engineering College, Maynooth University, Maynooth, Co. Kildare W23, Ireland
[3] Computer-Aided Design Department, St. Petersburg Electrotechnical University LETI, 5 Professora Popova St., 197022 Saint Petersburg, Russia
[4] School of Microelectronics and Control Engineering, Changzhou University, Changzhou 213159, People's Republic of China

E-mail: sangbo_76@163.com

Keywords: chameleon system, chaotic attractor, Hopf bifurcation, continuation diagram, bifurcation diagram, offset boosting

Abstract

This paper proposes a novel three-dimensional chameleon system derived from the classical Duffing oscillator. The innovation lies in transforming an externally driven Duffing system into an internally modulated autonomous system through a coupling between the driving force and system state. This coupling mechanism leads to a chameleon system with rich multistable dynamics. Through rigorous mathematical analysis, we establish the system's basic properties, including dissipativity, local stability and a supercritical Hopf bifurcation. Using a bifurcation diagram, for small values of parameter c, we detect that $c = 0$ serves as a critical boundary between hidden and self-excited chaotic regimes. Using a continuation diagram, we find that a supercritical Hopf bifurcation occurs at $c = 0$ followed by a period-doubling route to self-excited chaos as c increases. When $c = 0$, by varying two independent parameters, we conduct comprehensive bifurcation analysis, revealing intricate dynamical behaviors. A remarkable discovery is the system's ability to exhibit four nested hidden chaotic attractors, with their chaotic intensity (characterized by maximum Lyapunov exponents) monotonically decreasing from 0.1044 to 0.0226 as the distance from the equilibrium point increases. Additionally, we introduce an offset boosting mechanism that enables controlled shifting of attractors - a feature with potential applications in chaos-based engineering systems. The system is validated through numerical simulations and physical implementation using an electronic circuit that employs MC33078 and OPA2134 operational amplifiers with an 8th-order polynomial approximation of the cosine function.

1. Introduction

As a highly interdisciplinary field, chaos theory emerged from the study of nonlinear dynamical behaviors. In 1963, meteorologist Lorenz proposed a 3D nonlinear system for describing atmospheric motions. Chaotic systems exhibit several fundamental characteristics, such as their sensitivity to initial conditions, aperiodicity, and boundedness [1]. The study of chaos theory remains a vibrant and fascinating area within scientific research and engineering applications. Chaos has found applications across various fields, including economics [2], cryptography [3], robotics [4], among others.

Both bifurcation and continuation diagrams depict how the behavior of a dynamical system evolves as a control parameter varies. A bifurcation diagram is plotted by simulating the system from fixed initial conditions, discarding the transient behavior, and then calculating the intersections of the trajectory with a chosen plane in a specific direction. This process can be easily modified to generate a continuation diagram, where the initial condition for each simulation is set to the final value of the previous simulation. Compared to bifurcation diagrams, continuation diagrams allow for a more gradual exploration of the system's behavior as control

© 2025 IOP Publishing Ltd. All rights, including for text and data mining, AI training, and similar technologies, are reserved.

parameters change. Chaotic system control involves developing state feedback control laws to stabilize a dynamical system. When system parameters are uncertain, we can employ adaptive control techniques to achieve stabilization [5, 6]. Amplitude control refers to the ability to regulate the magnitude of a signal, typically in the context of chaotic systems. It was shown in [7] that symmetric chaotic systems can provide the possibility of multistability as well as an independent amplitude control parameter.

Leonov and Kuznetsov [8–10] introduced the classification of attractors as hidden or self-excited, in conjunction with the discovery of the hidden Chua attractor. They also developed a method that utilizes homotopy and numerical continuation to localize hidden attractors [11, 12]. A self-excited attractor refers to an attractor that has a basin of attraction that intersects with open neighborhoods that contain the equilibrium points of the dynamical system. Standard numerical methods can identify this type of attractor. On the other hand, a hidden attractor is an attractor whose basin of attraction does not intersect with any open neighborhoods containing the equilibrium points of the dynamical system. This implies that it cannot be numerically found using random initial conditions and demands special analytical-numerical procedures to locate its basin of attraction. Hidden attractors are important in engineering applications because they allow unexpected and potentially disastrous responses to perturbations in a structure like a bridge or an airplane wing [13, 14].

The Shilnikov theorems provide criteria for identifying self-excited chaotic attractors in 3D systems with unstable hyperbolic equilibria. As noted by Zhou and Chen [15], the chaotic attractors of Lorenz, Rössler, Chua, Chen, and many other systems are in the sense of Shilnikov, but not all chaotic attractors are of Shilnikov sense. Beyond the scope of Shilnikov theorems, many chaotic flows with various types of non-hyperbolic equilibria were introduced [16–18]. Li and Hai [19] introduced a three-dimensional robust chaotic system with two non-hyperbolic equilibrium points, exhibiting features of amplitude and position modulation. It is shown that the presence of linear terms is not essential in producing complex behaviors [20].

Jafari *et al* [21] presented a review for dissipative hidden chaotic flows, categorizing them into three types: systems with a stable equilibrium [22, 23], systems without equilibrium [24], and systems with an infinite number of equilibria [25]. Molaie *et al* [26] presented some chaotic systems with a unique stable equilibrium point; Jafari and Sprott [27] proposed nine hidden chaotic flows with a line equilibrium. Kumarasamy *et al* [28] examined the role of saddle-node bifurcations in the formation of hidden attractors. Antimononicity refers to the concurrent creation and destruction of periodic orbits in nonlinear dynamical systems, leading to inevitable reversals of bifurcation cascades [29]. For a family of jerk systems with a hyperbolic tangent function, Li *et al* [30] demonstrated the role of antimonotonicity in creating hidden attractors with a stable equilibrium. Dong *et al* [31] recently conducted numerical simulations and circuit experiments on a chaotic system without equilibrium, exploring its applications in synchronization, offset boosting control, and image encryption.

A chameleon system is a chaotic system that can transition between self-excited and hidden attractors based on the system parameters. Jafari *et al* [32] introduced a quadratic chameleon system, which significantly enhanced the understanding of chaotic attractors, particularly those that are hidden. Natiq *et al* [33] presented a chameleon system with a trigonometric nonlinear controller. Signing *et al* [34] introduced a chameleon cryptosystem that combines chameleon chaotic systems with dynamic DNA coding to enhance image encryption security through the use of chaotic sequences. Tiwari *et al* [35] recently introduced a class of quadratic chameleon systems that enable the coexistence of hidden chaotic attractors and conservative tori.

Multistability, referring to the coexistence of distinct attractors, is an inherent property of many nonlinear dynamical systems. Multistable dynamical systems are highly sensitive to noise, initial conditions, and parameters [36]. Although the coexistence of self-excited attractors can be found using standard computational methods, it is still difficult to identify the coexistence of hidden attractors in a system. Megastability refers to a scenario where a dynamical system has an infinite number of attractors that are countably infinite [37, 38]. Extreme multistability occurs when a dynamical system possesses an uncountably infinite number of attractors [39]. Leutcho *et al* [40] investigated periodic and chaotic patterns, hysteresis, and multistability in a single-gap terahertz split-ring resonator, offering key insights into nonlinear metamaterials and metasurfaces. Sambas *et al* [41] presented a 3D chaotic system with line equilibrium and multistability. Vijayakumar *et al* [42] explored a 4D hyper-jerk system with a unique equilibrium, which can generate different varieties of two, three, four, or five coexisting hidden and self-excited attractors. Vaidyanathan *et al* [43] introduced a 3D chaotic jerk system with a stable equilibrium and multistability. Benkouider *et al* [44] proposed a 4D hyperchaotic system with multistability. Sambas *et al* [45] introduced a 4D hyperjerk system with multistability.

A Hopf bifurcation is a type of local bifurcation in which a fixed point of a system loses stability and gives rise to a periodic solution. It occurs when a complex conjugate pair of eigenvalues of the linearised flow at an equilibrium point becomes purely imaginary. This bifurcation occurs in two forms: supercritical and subcritical. In the supercritical case, a stable equilibrium point transitions into a periodic orbit at the critical point. Conversely, in the subcritical case, a stable fixed point gives way to an unstable periodic solution. The latter situation poses a potential risk, as stable large-amplitude periodic orbits may coexist with the stable equilibrium

point [46]. Stankevich *et al* [9], Zhao *et al* [47] studied the dynamics of the Chua systems, establishing a connection between subcritical Hopf bifurcations of equilibria and the emergence of hidden attractors. Using a family of quadratic jerk systems, Liu *et al* [48] also shown that subcritical Hopf bifurcations are closely related to the emergence of hidden attractors.

The design of a chaotic system with independent non-bifurcation parameters faces a significant challenge due to the broadband random-like nature of chaos [49]. Offset-boosting involves adjusting the average value of a state variable by introducing a constant term into the system model, resulting in signal offset and enabling control of signal polarity. Li *et al* [50] proposed an offset-boosting based strategy for the identification of multistability in dynamical systems, employing nonbifurcation operations for the diagnosing of multistability. In chaotic and hyperchaotic systems [51, 52], offset boosting controls have been implemented, enabling direct offset regulation through the use of a single constant.

Yang *et al* [53] proposed a simple three-dimensional chaotic system characterized by a sinusoidal function, resulting in infinitely many equilibria. Ramar [54] presents a new chaotic system with three nonlinear terms and a sine term, highlighting its dynamics and potential for secure communication through adaptive synchronization and dc offset boosting control. Zhang *et al* [55] reported a chaotic system that generates controllable multi-scroll chaotic attractors with multiple wings and 2D grid-scroll behaviors by introducing a sine function.

Consider the Duffing equation

$$\ddot{x} + \gamma\dot{x} + \alpha x + \beta x^3 + F\cos(\omega t) = 0, \tag{1}$$

where x represents the displacement, γ is the damping coefficient, α and β are the linear and nonlinear stiffness coefficients, respectively, F is the amplitude of the driving force, and ω is the driving frequency. It is used to describe the hardening spring effect observed in many mechanical problems. The Duffing oscillator is well known for exhibiting the period-doubling phenomenon and self-excited chaotic dynamics. Duffing-like oscillators have practical applications in engineering and science, including biological systems [56], energy harvesting [57], and physics [58].

Let $y = -\dot{x}$ and $z = t$. Equation (1) becomes

$$\begin{cases} \frac{dx}{dt} &= -y, \\ \frac{dy}{dt} &= \alpha\, x - \gamma\, y + \beta\, x^3 + F\cos(\omega\, z), \\ \frac{dz}{dt} &= 1. \end{cases} \tag{2}$$

Let $\alpha = 1, \gamma = -c, \beta = 0, F = 1$. Replacing the constant in the third equation with $-a\,y - b\,z$, we obtain the following system

$$\begin{cases} \frac{dx}{dt} &= -y, \\ \frac{dy}{dt} &= x + c\, y + \cos(\omega\, z), \\ \frac{dz}{dt} &= -a\, y - b\, z, \end{cases} \tag{3}$$

where $a, b, \omega > 0$ and $c \in \mathbb{R}$. In the simplified case when $c = 0$, it consists of four linear terms and one cosine nonlinearity.

The introduction of ωz transforms the system from being externally driven (by $\cos(\omega t)$) to being internally modulated, where the driving force $\cos(\omega z)$ depends on the evolving state of the system. This coupling between the driving force and the system's state introduces more complex dynamical behaviors, as the driving force is no longer periodic or predictable but instead depends on the interplay between z, y, and x.

Compared to the Duffing self-excited chaotic oscillator, the autonomous system (3) is a chameleon system which exhibits multistability. Our innovation is twofold: first, we present an elegant chameleon system derived from the classical Duffing oscillator; second, we investigate the mechanisms underlying self-excited and hidden chaotic attractors, and the multistability within this novel system.

To compare the systems discussed in the papers [53–55] and the current work, we summarize their mathematical characteristics, attractors, and whether Hopf bifurcation analysis is addressed. Table 1 presents a comparison of the four systems.

The paper is organized as follows. In section 2, we explore the basic properties of system (3): including dissipativity, stability analysis and Hopf bifurcation. Section 3 presents an analysis of the chameleon phenomena for small c. By plotting a continuation diagram with respect to c, the next section demonstrates that the system transitions from a stable equilibrium to a periodic orbit and eventually to self-excited chaos via a supercritical Hopf bifurcation and a period-doubling cascade. Section 5 explores the rich hidden dynamics of the system when $c = 0$, using continuation diagrams to study the effects of varying parameters b and ω, employing a

Table 1. Comparison of systems in some papers and the current work.

Paper	Terms	Nonlinear functions	Attractors	Hopf bifurcation analysis
[53]	6 terms	One sine function	Self-excited chaotic attractors	Not discussed
[54]	7 terms	Three quadratic terms, One sine function	Self-excited chaotic attractors	Not discussed
[55]	7 terms	One sine function	Self-excited chaotic attractors	Not discussed
Current paper	6 terms	One cosine function	Self-excited and hidden chaotic attractors	Rigorously treated

bifurcation diagram to investigate the influence of initial conditions, particularly $y(0)$, and examining the dynamics of offset boosting by adding an extra constant k for the variable x in the second equation of the system. Section 6 presents the design and implementaion of an electronic circuit for a hidden chaotic system. In section 7, we provide a summary of the content presented in the paper.

2. Basic properities

This section is concerned with some basic properties of system (3).

2.1. Dissipativity

Consider a 3D vector field $\mathrm{F} = (F_1, F_2, F_3)$, where $F_1, F_2,$ and F_3 are the components of the vector field in the $x, y,$ and z directions, respectively. The divergence of F is a scalar measure of how much the vector field spreads out from a point. It is calculated using the formula:

$$\nabla \cdot \mathrm{F} = F_{1x} + F_{2y} + F_{3z}, \tag{4}$$

where $F_{1x}, F_{2y},$ and F_{3z} represent the partial derivatives of $F_1, F_2,$ and F_3 with respect to $x, y,$ and z, respectively.

Let $\mathrm{F} = (F_1, F_2, F_3)$ be the vector field associated to system (3). The divergence of F is

$$\nabla \cdot \mathrm{F} = F_{1x} + F_{2y} + F_{3z} = -(b - c). \tag{5}$$

Note that when $b > c$, system (3) is dissipative.

Let $V(t)$ be the volume that evolves with the flow, starting from the initial time $t = 0$. By the Liouville divergence theorem [59], we have

$$\frac{1}{V}\frac{dV}{dt} = \nabla \cdot \mathrm{F} = -(b - c). \tag{6}$$

Thus the volume $V(t)$ contracts exponentially in time as follows:

$$V(t) = V(0)\exp(-(b - c)t). \tag{7}$$

2.2. Stability analysis and Hopf bifurcation

System (3) has an equilbrium at $P_1 = (-1, 0, 0)$. The Jacobian matrix of the system at P_1 admits the following characteristic polynomial

$$g(\lambda) := \lambda^3 + (b - c)\lambda^2 + (1 - bc)\lambda + b. \tag{8}$$

From (8) and $b > 0$, using Routh-Hurwitz criterion, we know that the equilibrium is asymptotically stable if $c < 0$.

When $c = 0$, the equilibrium P_1 is non-hyperbolic with eigenvalues: $\lambda_{1,2} = \pm \mathrm{i}$ and $\lambda_3 = -b$. The local stability can be determined by Hopf bifurcation analysis.

Let $g(\lambda) = 0$. Using the implicit function theorem, we have

$$\mathrm{Re}\left(\frac{d\lambda}{dc}\bigg|_{c=0,\lambda=\pm\mathrm{i}}\right) = \frac{1}{2}. \tag{9}$$

This implies the transversality condition for the Hopf bifurcation at $c = 0$ is satisfied.

As a summary, a Hopf bifurcation of system (3) occurs from the equilibrium point P_1 at $c = 0$.

2.3. Supercritical Hopf bifurcation

Letting $c = 0$, system (3) becomes

$$\begin{cases} \frac{dx}{dt} &= -y, \\ \frac{dy}{dt} &= x + \cos(\omega z), \\ \frac{dz}{dt} &= -a\, y - b\, z, \end{cases} \tag{10}$$

where $a > 0$, $b > 0$ and $\omega > 0$. It is the so-called simplified case.

The Jacobian matrix of this system at $P_1 = (-1, 0, 0)$ takes the form

$$A = \begin{bmatrix} 0 & -1 & 0 \\ 1 & 0 & 0 \\ 0 & -a & -b \end{bmatrix}. \tag{11}$$

Let $\mathrm{P} = (\mathrm{Re}\,\mathrm{v}_1, -\mathrm{Im}\,\mathrm{v}_1, \mathrm{r}_3)$, where $\mathrm{v}_1, \mathrm{r}_3$ are the eigenvectors of the matrix A corresponding to $\lambda_1 = \mathrm{i}$ and $\lambda_3 = -b$,

$$\mathrm{v}_1 = \begin{bmatrix} \frac{1}{a} - \frac{b\,\mathrm{i}}{a} \\ -\frac{\mathrm{i}}{a} - \frac{b}{a} \\ 1 \end{bmatrix}, \quad r_3 = \begin{bmatrix} 0 \\ 0 \\ 1 \end{bmatrix}. \tag{12}$$

Let us introduce the transformation

$$\begin{bmatrix} x \\ y \\ z \end{bmatrix} = P \cdot \begin{bmatrix} u \\ v \\ w \end{bmatrix} + \begin{bmatrix} -1 \\ 0 \\ 0 \end{bmatrix}. \tag{13}$$

This leads to

$$\begin{cases} x &= -1 + \frac{1}{a}\, u + \frac{b}{a}\, v, \\ y &= -\frac{b}{a}\, u + \frac{1}{a}\, v, \\ z &= u + w. \end{cases} \tag{14}$$

By applying this transformation, system (10) becomes

$$\begin{cases} \frac{du}{dt} &= -v + \frac{ab\omega^2 u^2}{2(b^2+1)} + \frac{ab\omega^2 uw}{b^2+1} + \frac{ab\omega^2 w^2}{2(b^2+1)} + \cdots, \\ \frac{dv}{dt} &= u - \frac{a\omega^2 u^2}{2(b^2+1)} - \frac{a\omega^2 uw}{b^2+1} - \frac{a\omega^2 w^2}{2(b^2+1)} + \cdots, \\ \frac{dw}{dt} &= -bw - \frac{ab\omega^2 u^2}{2(b^2+1)} - \frac{ab\omega^2 uw}{b^2+1} - \frac{ab\omega^2 w^2}{2(b^2+1)} + \cdots. \end{cases} \tag{15}$$

Using the formula presented in [60], the first focus quantity (also known as Lyapunov constant) of system (15) is obtained as follows:

$$W_1 = -\frac{a^2 b\, \omega^4}{8(b^2+4)(b^2+1)}, \tag{16}$$

which is always negative.

Based on the signs of (9) and (16), we can conclude that the Hopf bifurcation at $c = 0$ is supercritical, resulting in the emergence of a stable periodic attractor for $c > 0$. This also implies that the unique equilibrium $P_1 = (-1, 0, 0)$ is always stable at $c = 0$.

3. Chameleon chaotic dynamics for small c when $(a, b, \omega) = (7, 0.8, 1)$

Let $a = 7$, $b = 0.8$, and $\omega = 1$. For system (3), with the fixed initial conditions $(x(0), y(0), z(0)) = (-4, 0, 0)$, the bifurcation diagram and Lyapunov exponent spectrum with respect to c are shown in figure 1. Starting from $c = 0.013$, as the value of c decreases, the system undergoes a period-doubling route to chaos. Eventually, as c continues to decrease, the system transitions to a steady state at $x = -1$, $y = 0$, and $z = 0$. The bifurcation diagram closely correlates with the Lyapunov exponent spectrum.

For $c = -0.0042$, 0, and 0.0076, figure 2 shows the projections of three strange attractors onto the (x, y)-plane, with the initial conditions $(x(0), y(0), z(0)) = (-4, 0, 0)$. For cases $c = -0.0042$ and $c = 0$, there exists a hidden chaotic attractor, coexisting with a stable equilibrium (green star). For case $c = 0.0076$, there exists a self-

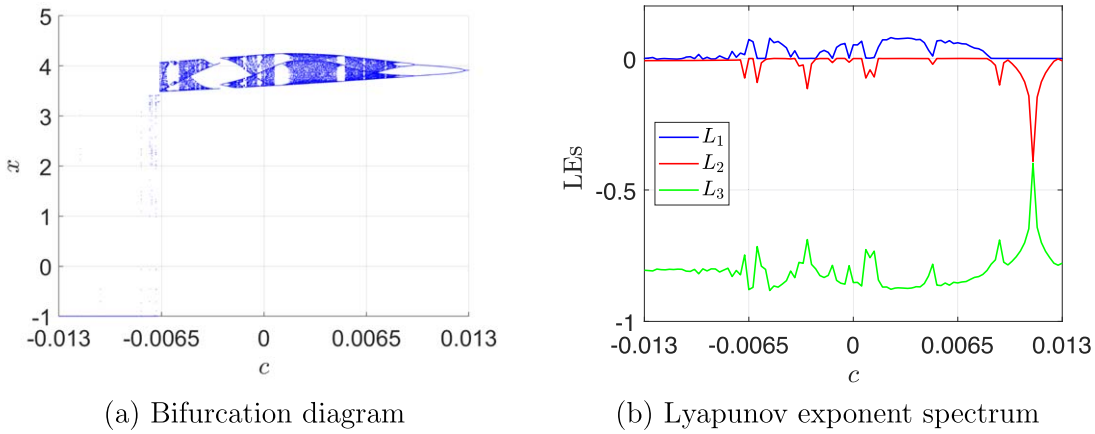

(a) Bifurcation diagram (b) Lyapunov exponent spectrum

Figure 1. Bifurcation diagram and Lyapunov exponent spectrum of system (3) with respect to c for $(a, b, \omega) = (7, 0.8, 1)$. Initial conditions: $(x(0), y(0), z(0)) = (-4, 0, 0)$.

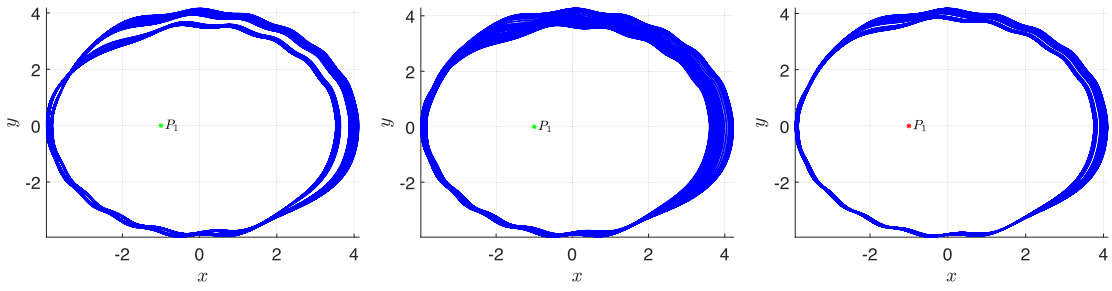

(a) $c = -0.0042$ (b) $c = 0$ (c) $c = 0.0076$

Figure 2. Projections of chaotic attractors on the (x, y)-plane for system (3) with $(a, b, \omega) = (7, 0.8, 1)$. (a) $c = -0.0042$, (b) $c = 0$, (c) $c = 0.0076$. Green stars correspond to the stable equilibrium: $(-1, 0, 0)$. Red star corresponds to the unstable equilibrium: $(-1, 0, 0)$. Initial conditions: $(x(0), y(0), z(0)) = (-4, 0, 0)$.

Table 2. Basic properties of system (3) with $(a, b, \omega) = (7, 0.8, 1)$ for $c = -0.0042, 0$, and 0.0076. Initial conditions: $(-4, 0, 0)$.

Parameter	Equilibrium	Eigenvalues	LEs	D_{KY}	Chaotic type
$c = -0.0042$	$(-1, 0, 0)$	$\lambda_{1,2} = -0.0021 \pm i$ $\lambda_3 = -0.8$	$L_1 = 0.0388$ $L_2 = 0$ $L_3 = -0.8429$	2.046	Hidden
$c = 0$	$(-1, 0, 0)$	$\lambda_{1,2} = \pm i$ $\lambda_3 = -0.8$	$L_1 = 0.0563$ $L_2 = 0$ $L_3 = -0.8563$	2.066	Hidden
$c = 0.0076$	$(-1, 0, 0)$	$\lambda_{1,2} = 0.0038 \pm i$ $\lambda_3 = -0.8$	$L_1 = 0.0384$ $L_2 = 0$ $L_3 = -0.8309$	2.046	Self-excited

excited chaotic attractor, coexisting with an unstable equilibrium (red star). This suggests that $c = 0$ is the critical point where the system's attractor type undergoes a transition.

For these cases, the Lyapunov exponents (LEs), Kaplan-Yorke dimensions (D_{KY}) and the eigenvalues ($\lambda_{1,2,3}$) of the unique equilibrium are shown in table 2.

4. Self-excited chaotic regime from a supercritical Hopf bifurcation when $(a, b, \omega) = (7, 0.8, 1)$

Let $a = 7$, $b = 0.8$ and $\omega = 1$. Starting from the initial conditions $(x(0), y(0), z(0)) = (-0.81, -0.06, 0.39)$, the continuation diagram and Lyapunov exponent spectrum of system (3) obtained by varying from $c = -0.01$ to

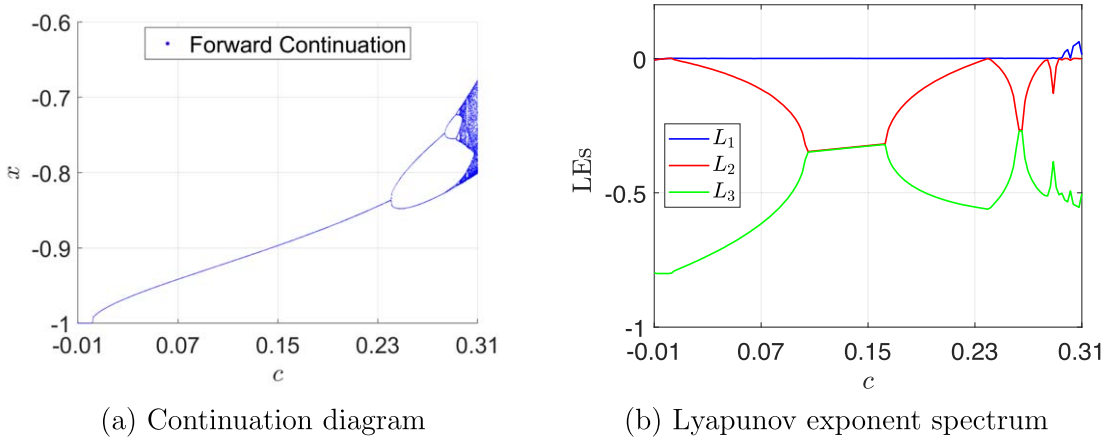

(a) Continuation diagram (b) Lyapunov exponent spectrum

Figure 3. Continuation diagram and Lyapunov exponent spectrum for system (3) obtained by varying c from $c = -0.01$ to $c = 0.31$ and setting $(a, b, \omega) = (7, 0.8, 1)$. Starting point at $c = -0.01$: $(x(0), y(0), z(0)) = (-0.81, -0.06, 0.39)$.

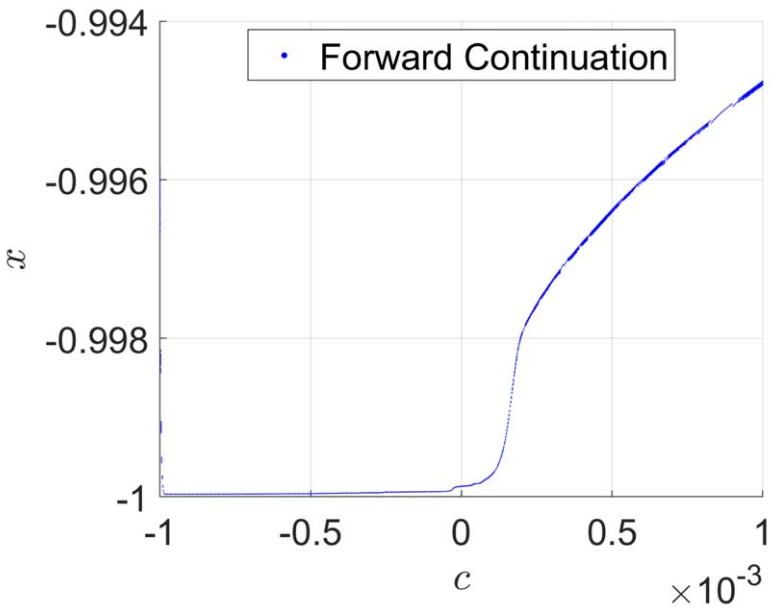

Figure 4. Continuation diagram for system (3) obtained by varying c from $c = -0.001$ to $c = 0.001$ and setting $(a, b, \omega) = (7, 0.8, 1)$. Starting point at $c = -0.001$: $(x(0), y(0), z(0)) = (-0.81, -0.06, 0.39)$.

$c = 0.31$ are shown in figure 3. For $c \in [-0.01, 0)$, the orbit of the system is attracted to the steady state at $P_1 = (-1, 0, 0)$. At $c = 0$, a supercritical Hopf bifurcation occurs, yielding a stable periodic cycle for $c > 0$. With further increase of c, the system experiences a period-doubling route to self-excited chaos.

By the way, the presence of a supercritical Hopf bifurcation at $c = 0$ can be observed in the continuation diagram when c is small, see also the zoomed-in version in figure 4.

Using the initial conditions $(x(0), y(0), z(0)) = (-0.81, -0.06, 0.39)$, figure 5 depicts the self-excited chaotic attractor of system (3) for $(a, b, c, \omega) = (7, 0.8, 0.31, 1)$, along with its projections onto the (x, y), (y, z) and (x, z) planes. The Lyapunov exponents of the strange attractor are $(0.0057, 0, -0.4949)$. The Kaplan-Yorke dimension is 2.011. The Jacobian matrix at the equilibrium $P_1 = (-1, 0, 0)$ has eigenvalues $\lambda_{1,2} = 0.1550 \pm 0.9879$ i and $\lambda_3 = -0.8$. This implies that the unique equilibrium P_1 is a saddle-focus of index 2.

5. Simplified case: hidden dynamics of system (3) with $(a, c) = (7, 0)$

This section explores the hidden dynamics of system (3) with $(a, c) = (7, 0)$, focusing on the effects of varying parameters (b, ω) and initial conditions.

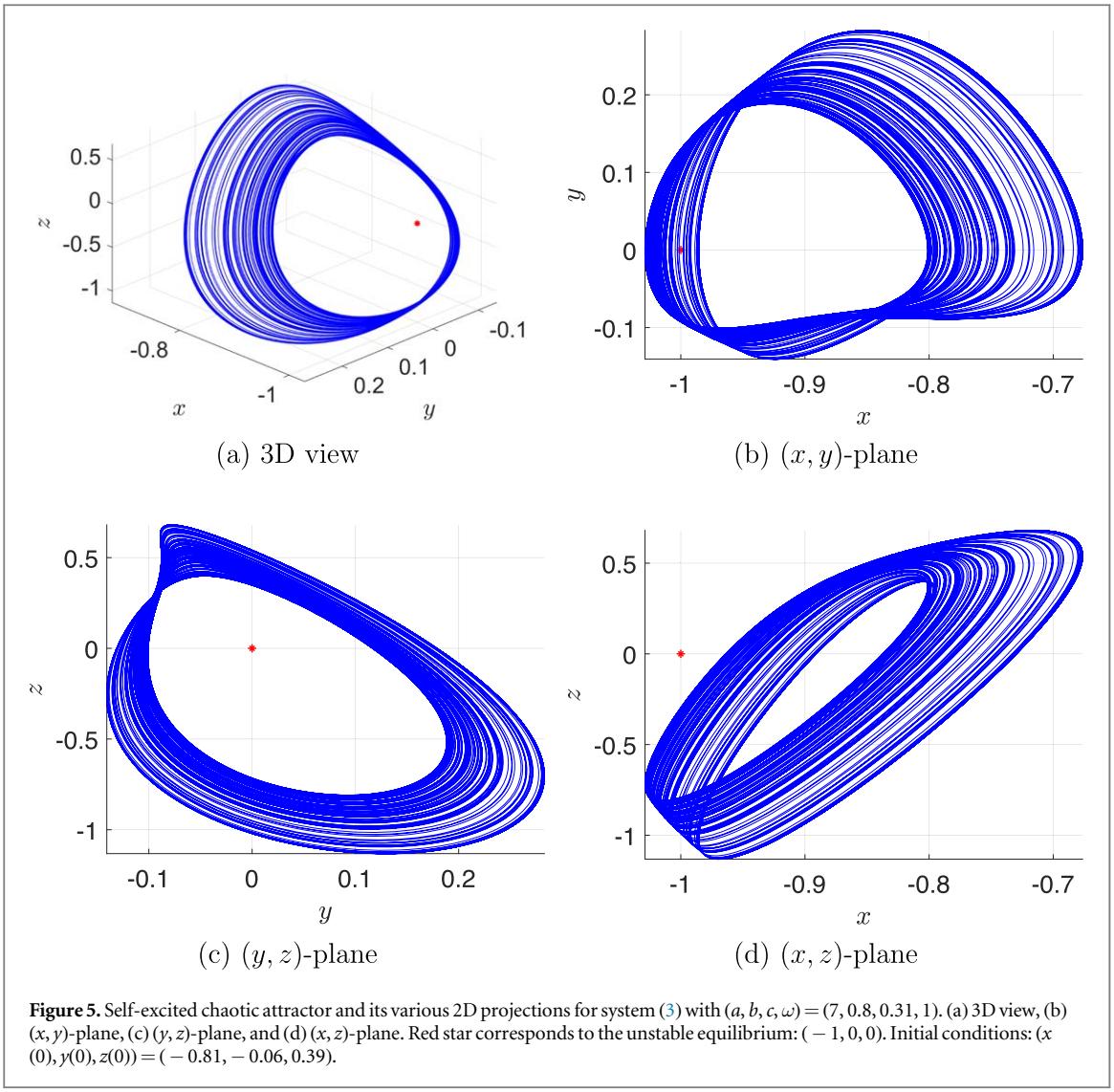

Figure 5. Self-excited chaotic attractor and its various 2D projections for system (3) with $(a, b, c, \omega) = (7, 0.8, 0.31, 1)$. (a) 3D view, (b) (x, y)-plane, (c) (y, z)-plane, and (d) (x, z)-plane. Red star corresponds to the unstable equilibrium: $(-1, 0, 0)$. Initial conditions: $(x(0), y(0), z(0)) = (-0.81, -0.06, 0.39)$.

5.1. Hidden dynamics by varying b with $(a, c, \omega) = (7, 0, 1)$

Let $a = 7$, $c = 0$, and $\omega = 1$. For $b \neq 0$, system (3) always has a non-hyperbolic, stable equilibrium at $P_1 = (-1, 0, 0)$. To explore the hidden chaotic dynamics of the system, we will vary b within the range $[0, 1.67]$.

Using two initial values $(0, 0, 3)$ and $(0, 0, 4)$, the forward (blue) and backward (red) continuation diagrams and the Lyapunov exponent spectra of the system with respect to parameter b are plotted in figure 6. With an increase in b, the orbit starting from $(0, 0, 3)$ undergoes period-doubling cascades to chaos. At high values of b, the system returns to a periodic state. With a decrease in b, a similar process is observed for the orbit starting from $(0, 0, 4)$.

For two typical values of b, the phase portraits of the system are shown in figure 7. For $b = 0.45$, from inside to outside, there is a point attractor (red), a hidden chaotic attractor (green), two period-2 orbits (blue and yellow), four period-1 orbits (magenta, cyan, dark red, and dark green). For $b = 1.04$, from inside to outside, there is a point attractor (red), two hidden chaotic attractors (blue and yellow), two period-2 orbits (magenta and cyan).

In the $z = 0$ plane, the basins of attraction corresponding to the attractors in figure 7 are shown in figure 8, using the same color schemes. Table 3 provides detailed information about the hidden chaotic attractors for $b = 0.45$ and $b = 1.04$.

5.2. Hidden dynamics by varying ω when $(a, b, c) = (7, 0.8, 0)$

Let $a = 7$, $b = 0.8$, and $c = 0$. System (3) always has a non-hyperbolic, stable equilibrium at $P_1 = (-1, 0, 0)$. To explore the hidden chaotic dynamics of the system, we will vary ω within the range $[0.8, 1.8]$.

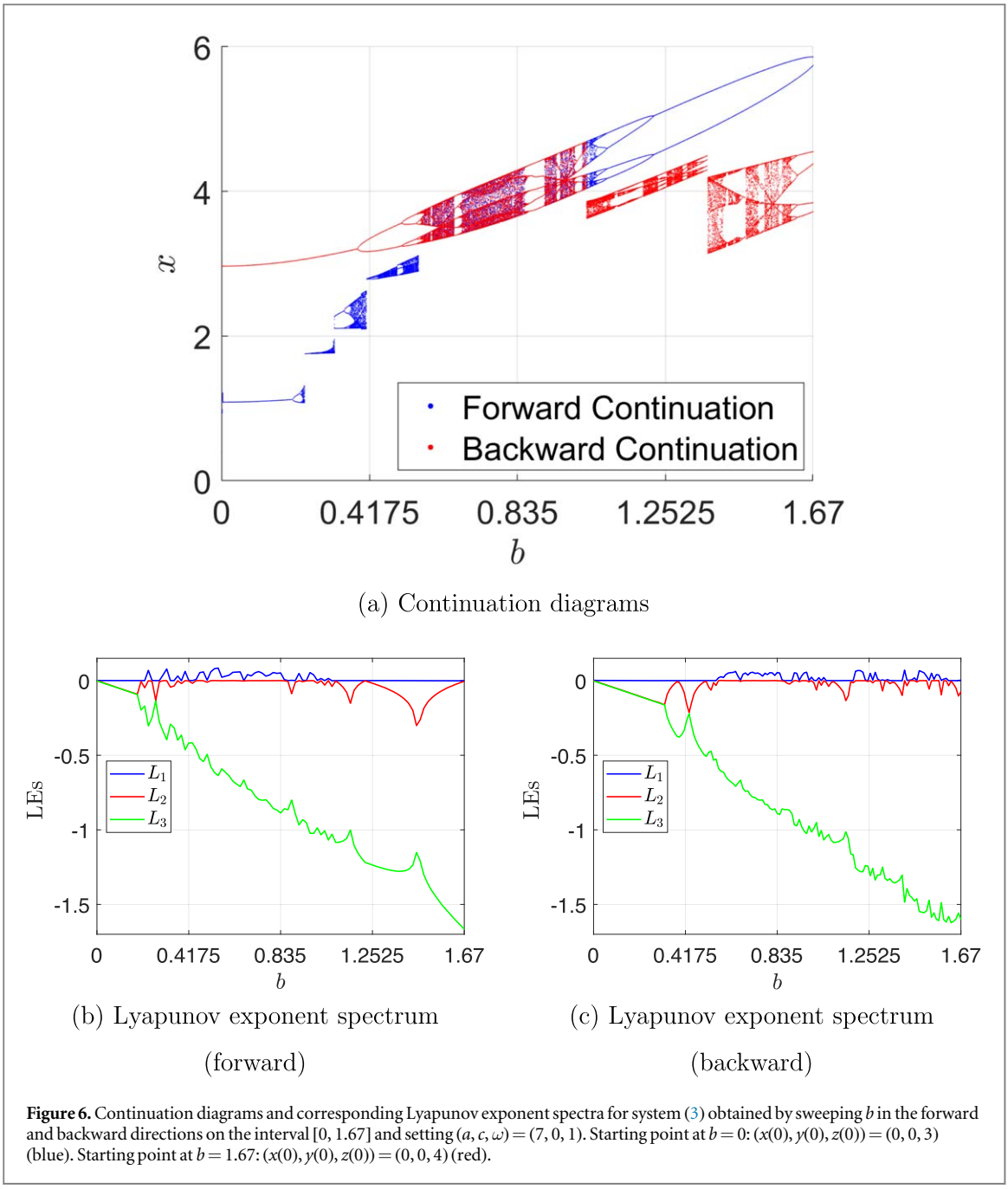

(a) Continuation diagrams

(b) Lyapunov exponent spectrum (forward)

(c) Lyapunov exponent spectrum (backward)

Figure 6. Continuation diagrams and corresponding Lyapunov exponent spectra for system (3) obtained by sweeping b in the forward and backward directions on the interval [0, 1.67] and setting $(a, c, \omega) = (7, 0, 1)$. Starting point at $b = 0$: $(x(0), y(0), z(0)) = (0, 0, 3)$ (blue). Starting point at $b = 1.67$: $(x(0), y(0), z(0)) = (0, 0, 4)$ (red).

5.2.1. Continuation diagram with respect to ω

Starting from the initial conditions $(x(0), y(0), z(0)) = (0, 6, 0)$, the continuation diagram and Lyapunov exponent spectrum of system (3), obtained by varying ω from 0.8 to 1.8, are shown in figure 9. A period-doubling route to chaos can be observed for lower values of ω. At $\omega \approx 1.1$, the system transitions into a chaotic regime. As ω increase further, the chaotic regimes are intermittently disrupted by interior crises and periodic windows. Overall, the system exhibits a broad range of chaos.

5.2.2. Bifurcation diagram with respect to $y(0)$ *at* $\omega = 1.74$

Let $\omega = 1.74$. As $y(0)$ varies, we will use numerical methods to show that the system can exhibit multistability. Figure 10 presents the bifurcation diagram and Lyapunov exponent spectrum of the system with respect to $y(0)$, constructed using the local maximal method for the initial conditions $(x(0), y(0), z(0)) = (0, y(0), 0)$, where $6 \leqslant y(0) \leqslant 9$.

Let

$$(y_1, \cdots, y_9) = (6,\ 6.5,\ 7,\ 7.26,\ 7.5,\ 8.03,\ 8.22,\ 8.5,\ 8.8). \tag{17}$$

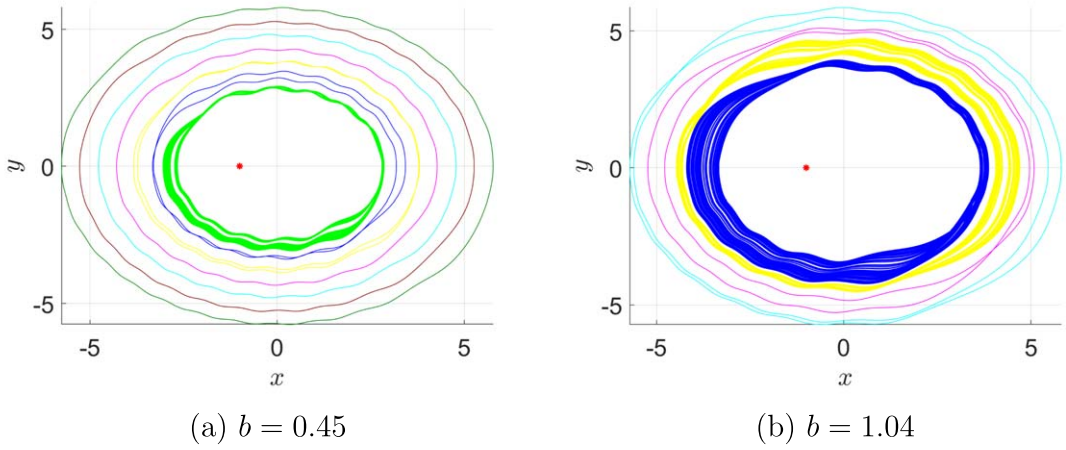

Figure 7. Coexisting attractors in system (3) with $(a, c, \omega) = (7, 0, 1)$. (a) $b = 0.45$, initial conditions: $(x(0), y(0), z(0)) = (0, 0, 0)$ (red), $(-1.6, -1.8, 0)$ (green), $(-2.1, -2.3, 0)$ (blue), $(-2.3, -2.7, 0)$ (yellow), $(-2.6, -3.0, 0)$ (magenta), $(-2.9, -3.4, 0)$ (cyan), $(-3.3, -3.7, 0)$ (dark red), $(-3.9, -3.9, 0)$ (dark green). (b) $b = 1.04$, initial conditions: $(x(0), y(0), z(0)) = (0, 0, 0)$ (red), (2.0, 2.4, 0) (blue), (3.0, 3.0, 0) (yellow), (3.6, 3.6, 0) (magenta), (3.8, 3.8, 0) (cyan).

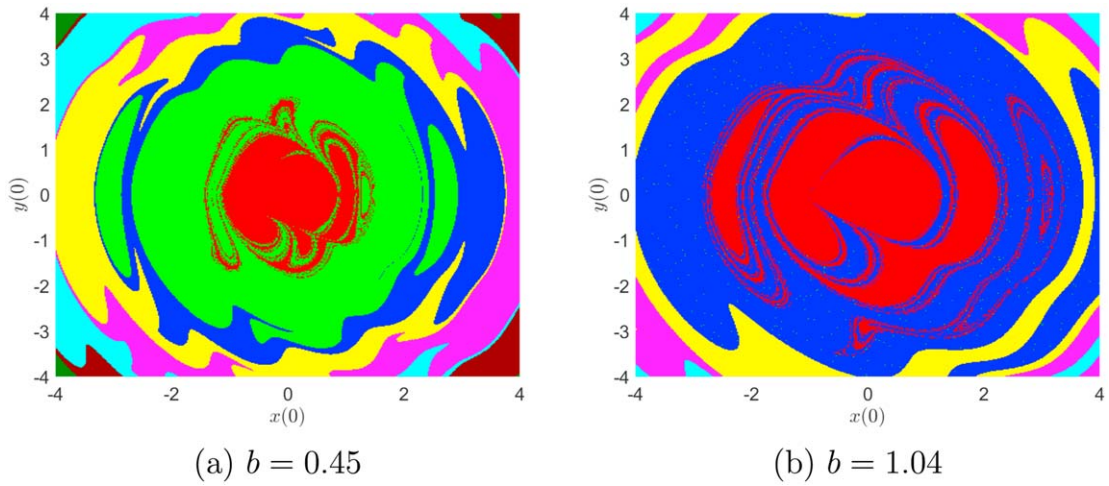

Figure 8. Basins of attraction for system (3) with $(a, c, \omega) = (7, 0, 1)$ in the $z = 0$ plane. (a) $b = 0.45$, (b) $b = 1.04$.

Table 3. Hidden chaotic attractors for system (3) with $(a, c, \omega) = (7, 0, 1)$ for $b = 0.45$ and $b = 1.04$.

Case	Equilibrium	Eigenvalues	Initial Conditions	LEs	D_{KY}	Chaotic Type
$b = 0.45$	$(-1, 0, 0)$	$\lambda_{1,2} = \pm i$ $\lambda_3 = -0.45$	$(-1.6, -1.8, 0)$	$L_1 = 0.0294$ $L_2 = 0$ $L_3 = -0.4795$	2.061	Hidden
$b = 1.04$	$(-1, 0, 0)$	$\lambda_{1,2} = \pm i$ $\lambda_3 = -1.04$	(2.0, 2.4, 0)	$L_1 = 0.0949$ $L_2 = 0$ $L_3 = -1.1350$	2.083	Hidden
			(3.0, 3.0, 0)	$L_1 = 0.0190$ $L_2 = 0$ $L_3 = -1.0586$	2.017	

For each k, we plot the attractor emanating from $Q_k := (0, y_k, 0)$. As shown in figure 11, a nested arrangement of these attractors is clearly visible, with the hidden chaotic attractors occupying the inner regions and the periodic solutions forming the outer layers. The hidden chaotic attractors associated with Q_1, Q_2, Q_3, and Q_4 are colored blue, green, red, and magenta, respectively. The remaining five initial conditions Q_5 to Q_9 correspond to periodic solutions, with colors assigned as cyan, yellow, purple, olive, and gray, respectively. In the plane $z = 0$, figure 12 shows the respective basins of attraction for the attractors in figure 11 with the same colors.

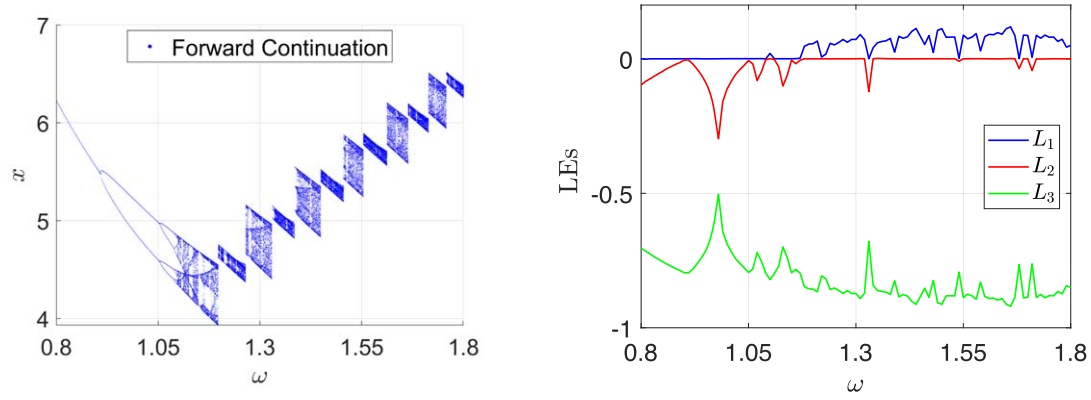

(a) Continuation diagram (b) Lyapunov exponent spectrum

Figure 9. Continuation diagram and Lyapunov exponent spectrum for system (3) obtained by varying ω from $\omega = 0.8$ to $\omega = 1.8$ with $(a, b, c) = (7, 0.8, 0)$. Starting point at $\omega = 0.8$: $(x(0), y(0), z(0)) = (0, 6, 0)$.

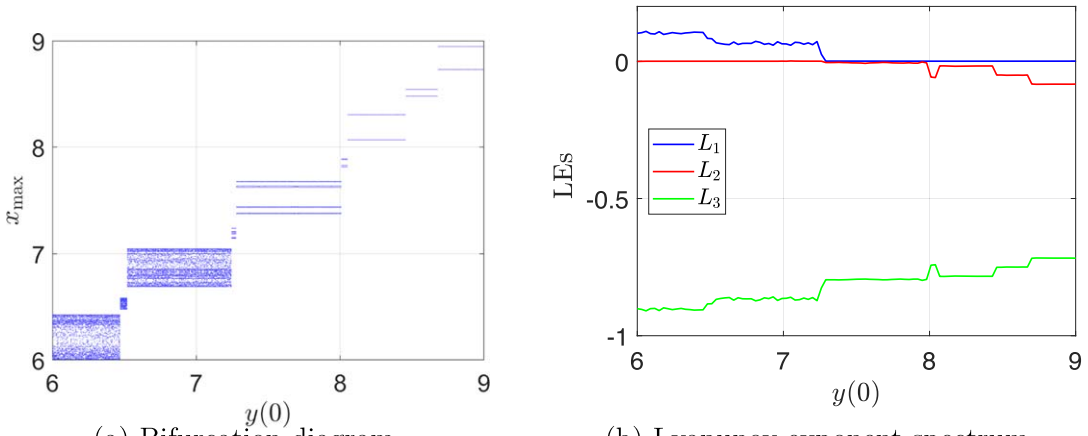

(a) Bifurcation diagram (b) Lyapunov exponent spectrum

Figure 10. Bifurcation diagram and Lyapunov exponent spectrum for system (3) with respect to initial condition $y(0)$ when $(a, b, c, \omega) = (7, 0.8, 0, 1.74)$. Initial conditions: $(x(0), y(0), z(0)) = (0, y(0), 0)$, where $6 \leqslant y(0) \leqslant 9$.

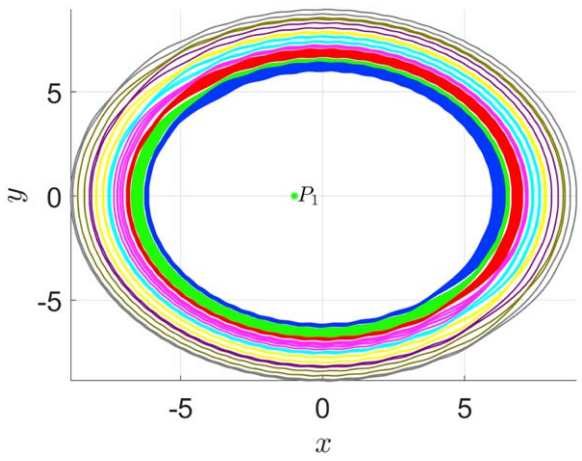

Figure 11. Projections of attractors on the (x, y)-plane for system (3) with $(a, b, c, \omega) = (7, 0.8, 0, 1.74)$. Initial conditions: $Q_k = (0, y_k, 0)$, where y_k are defined by (17) and $1 \leqslant k \leqslant 9$. Hidden chaotic attractors associated with Q_1, Q_2, Q_3, and Q_4 are colored blue, green, red, and magenta, respectively. Periodic solutions corresponding to Q_5 to Q_9 are shown in cyan, yellow, purple, olive, and gray, respectively. P_1 (green) represents the stable equilibrium at $(-1, 0, 0)$.

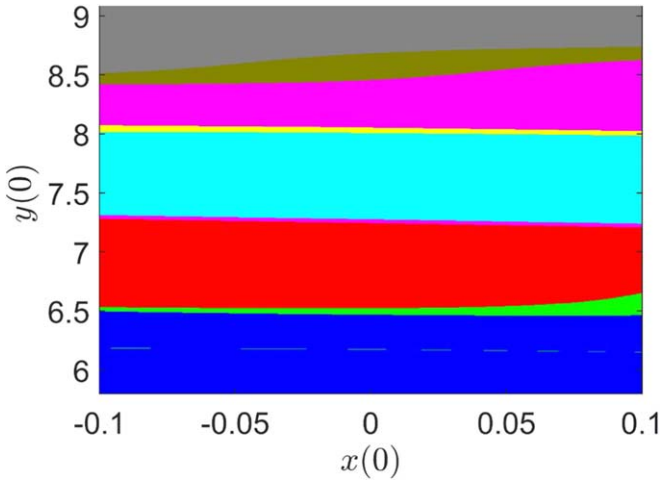

Figure 12. Basins of attraction for system (3) with $(a, b, c, \omega) = (7, 0.8, 0, 1.74)$ in the $z = 0$ plane.

Table 4. Properties of four hidden chaotic attractors in system (3) with parameters $(a, b, c, \omega) = (7, 0.8, 0, 1.74)$.

Equilibrium	Eigenvalues	Initial Data	LEs	D_{KY}	Chaotic type
$(-1, 0, 0)$	$\lambda_{1,2} = \pm i$ $\lambda_3 = -0.8$	$(0, 6, 0)$	$L_1 = 0.1044$ $L_2 = 0$ $L_3 = -0.9040$	2.115	Hidden
		$(0, 6.5, 0)$	$L_1 = 0.0882$ $L_2 = 0$ $L_3 = -0.8887$	2.099	
		$(0, 7, 0)$	$L_1 = 0.0692$ $L_2 = 0$ $L_3 = -0.8693$	2.079	
		$(0, 7.26, 0)$	$L_1 = 0.0226$ $L_2 = 0$ $L_3 = -0.8231$	2.027	

Table 4 provides detailed information about the four coexisting hidden chaotic attractors in the system. The maximum Lyapunov exponents L_1 of the nested hidden chaotic attractors surrounding the equilibrium point $(-1, 0, 0)$ decrease from 0.1044 to 0.0226 as one moves outward, indicating a reduction in the system's chaotic behavior with increasing distance from the equilibrium.

5.3. Offset boosting dynamics with $(a, b, c, \omega) = (7, 0.8, 0, 1.74)$

Offset boosting can be realized by incorporating an additional parameter into a state variable that is uniquely present in the system's mathematical formulation. This new parameter is crucial for adjusting the positions of the system's attractors.

The following system (18) is obtained from (3) by adding a new parameter k to the state variable x, resulting in the following set of equations:

$$\begin{cases} \frac{dx}{dt} &= -y, \\ \frac{dy}{dt} &= (x + k) + c\, y + \cos(\omega\, z), \\ \frac{dz}{dt} &= -a\, y - b\, z. \end{cases} \tag{18}$$

Let $a = 7$, $b = 0.8$, $c = 0$, and $\omega = 1.74$. For $k = -5, 0, 5$, the plots of time series for the x variable and 2D projections of the attractors are presented in figure 13, from which we can see that as the parameter k increases, the system's attractor shifts along the negative direction of the x-axis.

6. Circuit realization for a mathematical model

This section presents the physical implementation of a mathematical model through an electronic circuit.

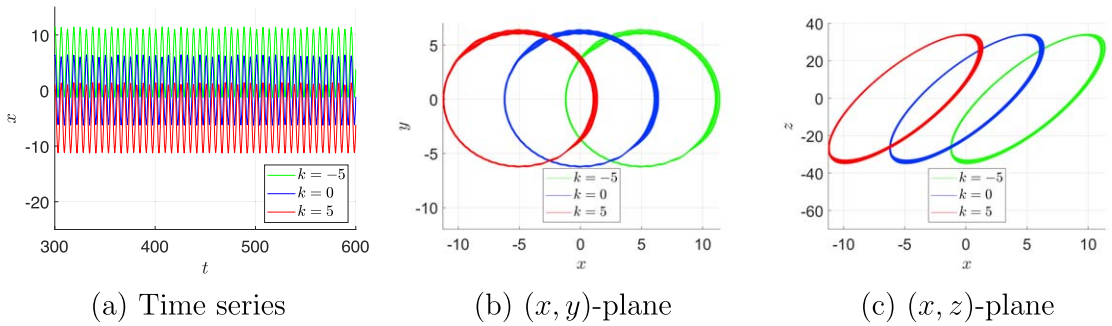

Figure 13. Dynamics of system (18) with $(a, b, c, \omega) = (7, 0.8, 0, 1.74)$ and varying parameter k. (a) Time series. (b) 2D projections of the attractors in the (x, y)-plane. (c) 2D projections of the attractors in the (x, z)-plane. Initial conditions: (5, 6, 0) (green), (0, 6, 0) (blue), $(-5, 6, 0)$ (red).

6.1. Mathematical model and circuit design

Let $a = 4.9$, $b = 3.5$, $c = 0$, and $\omega = 2$ in system (3), we get the following system:

$$\begin{cases} \frac{dx}{dt} &= -y, \\ \frac{dy}{dt} &= x + \cos(2z), \\ \frac{dz}{dt} &= -4.9\, y - 3.5\, z. \end{cases} \tag{19}$$

The system can exhibit three distinct types of behaviors depending on the initial conditions. The point attractor is generated from initial conditions (0, 0.2, 0), the hidden chaotic attractor from initial conditions (0, 2, 0), and the periodic attractor from initial conditions (0, 3, 0). The hidden chaotic attractor has Lyapunov exponents $L_1 = 0.0754$, $L_2 = 0$, and $L_3 = -3.5756$. Consequently, the Kaplan-Yorke dimension is calculated to be 2.021.

The corresponding circuit system can be designed as:

$$\begin{cases} \frac{dx}{dt} &= -\frac{1}{R_1 C_1} y, \\ \frac{dy}{dt} &= \frac{1}{R_2 C_2} x + \frac{1}{R_3 C_2} \cos\left(\frac{R_7}{R_6} z\right), \\ \frac{dz}{dt} &= -\frac{1}{R_4 C_3} y - \frac{1}{R_5 C_3} z. \end{cases} \tag{20}$$

By comparing systems (19) and (20), we obtain the relationships:

$$\frac{1}{R_1 C_1} : \frac{1}{R_2 C_2} : \frac{1}{R_3 C_2} : \frac{1}{R_4 C_3} : \frac{1}{R_5 C_3} = 1 : 1 : 1 : 4.9 : 3.5, \quad \omega = \frac{R_7}{R_6} = 2. \tag{21}$$

As a result, the resistors R_4, R_5, and R_7 are introduced as variable resistors, with their resistance values set to $R_4 = 20.4\ \text{k}\Omega$, $R_5 = 28.6\ \text{k}\Omega$, and $R_7 = 20\ \text{k}\Omega$, respectively. The fixed resistors R_1, R_2, and R_3 are each set to 100 kΩ, while the fixed resistor R_6 is set to 10 kΩ. Additionally, the capacitor values are defined as $C_1 = C_2 = C_3 = 10$ nF. The previously unmentioned resistor values R_8, R_9, $\cdots$, and R_{11} are set to 100 kΩ.

For system (20), the schematic circuit diagram built by Multisim is shown in figure 14. It is composed of five MC33078 operational amplifiers, eleven resistors (three variable and eight fixed), three capacitors, and three switches.

The X-coordinate equation is implemented through an integrator built around operational amplifier U_1, with input resistor R_1 (100 kΩ) and integration capacitor C_1 (10nF). The Y-coordinate processing incorporates two input paths: the X signal through R_2 (100 kΩ) and the cosine function output through R_3 (100 kΩ). These signals are integrated using operational amplifier U_3 with capacitor C_2 (10nF). Additional scaling is provided by R_8 and R_9 (both 100 kΩ), with inverting amplifier U_4 delivering the Y output.

The Z-coordinate circuit processes the Y input through variable resistor R_4 (100 kΩ, adjusted to 20.4%) and includes Z feedback through R_5 (100 kΩ, set to 28.6%). Integration is performed by operational amplifier U_5 with capacitor C_3 (10nF), with the followed inverting using amplifier U_6. The cosine function is implemented through a dedicated block (HB 1) with input scaling provided by R_6 (10 kΩ) and variable resistor R_7 (20 kΩ), establishing the required $\omega = 2$ scaling factor through the ratio R_7/R_6.

The circuit design incorporates switches $S_1 - S_3$ and regulated voltage source V_1 for setting initial conditions $(x(0), y(0), z(0)) = (0, V_1, 0)$. The relatively slow response time of the circuit enables manual initialization using these push-button switches.

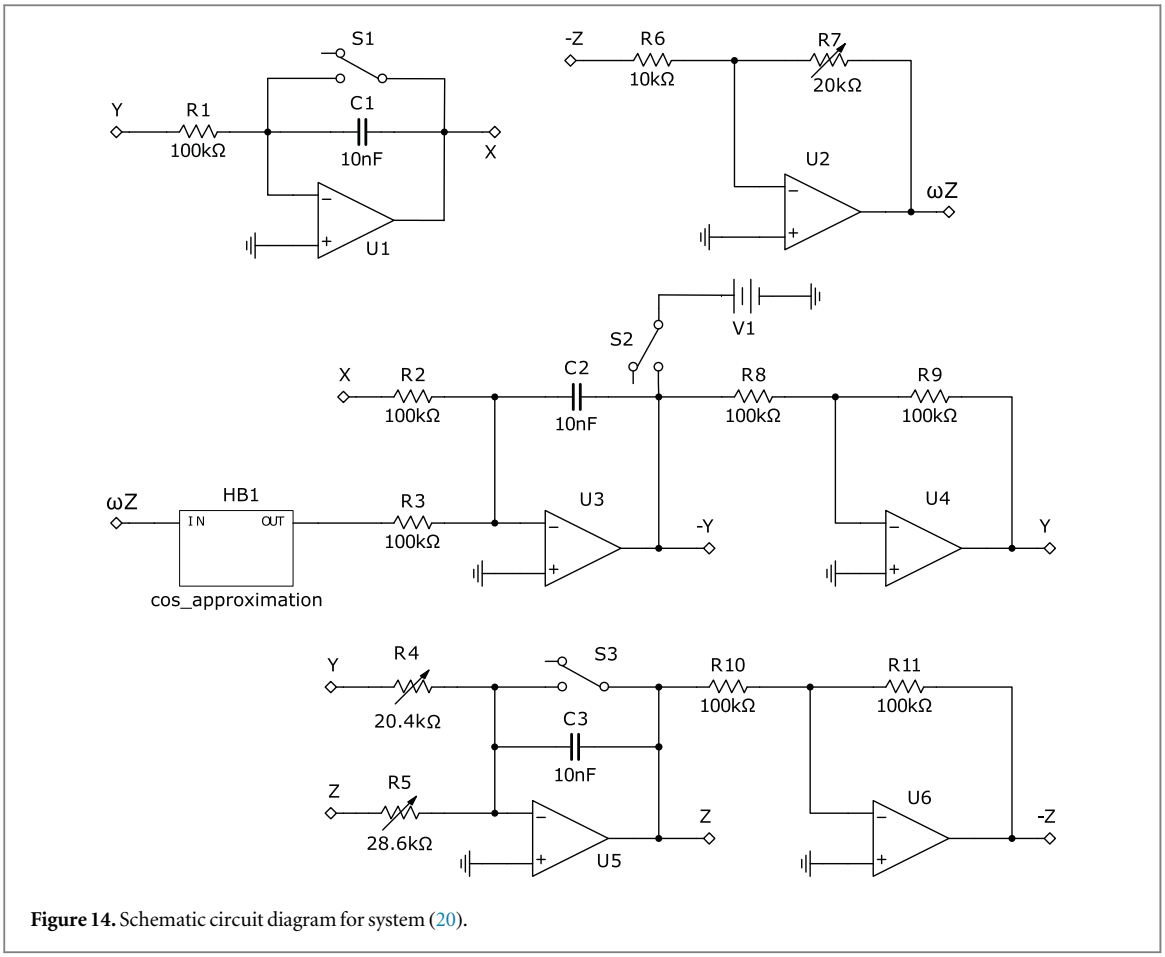

Figure 14. Schematic circuit diagram for system (20).

6.2. Cosine function approximation

The hardware approximation of the cosine function is an important part of the circuit realization. Observations of the dynamics from the model show that the cosine approximation block must simulate at least three cosine periods to preserve the rich dynamics inherent in the original system.

For the 4th order approximation, the following relation is implemented, with a root-mean-square error (RMSE) $\epsilon = 0.066$ for $x \in [-1.25\pi, 1.25\pi]$:

$$\cos(x) \approx (0.14x^2 - 1.419)^2 - 1.09.$$

To observe multiple coexisting attractors in the circuit, it is necessary to increase the order of approximation, as a minimum of three cosine periods is required for this purpose. Adding nested sums of squares and constants extends the range of the input values x. For example, the approximation by 8th order polynomial with RMSE $\epsilon = 0.132$ for $x \in [-2.5\pi, 2.5\pi]$ is as follows:

$$\cos(x) \approx ((-0.04x^2 + 1.67)^2 - 1.46)^2 - 0.933.$$

As shown in figure 15, the hardware implementation employs three AD633JN analog multipliers (A_1, A_2, A_3) with specific scaling factors: A_1 with 0.1V/V, and A_2, A_3 with −0.1 V/V. The circuit incorporates fixed resistors R_1 (30 kΩ), R_2, R_4, R_6 (10 kΩ each), R_9 (1 kΩ), $R_{10}, R_{11}, R_{12}, R_{15}$ (11 kΩ each), along with variable resistors R_3 (50 kΩ at 69%), R_7 (25 kΩ at 75%), R_8 (2 kΩ at 48%), R_{13} (100 kΩ at 85%), R_{14} (100 kΩ at 65%), and R_5 (100 kΩ at 50%).

The operational amplifiers are implemented using MC33078 (U_1 through U_5) for the main signal processing stages and OPA2134 (U_6) for the output stage. The first stage with U_1 processes the initial polynomial term $p_1 = (-0.04x^2 + 1.67)$, followed by U_2 computing $p_2 = p_1^2 - 1.46$. The amplifier U_5 with diodes D_1 and D_2 implements the reflection of polynomial branches, while diodes $D_3 - D_6$ provide amplitude limiting below 1.2V. The circuit operates with dual power supply ±15V. Op amp U_7 acts as voltage follower. Although the multiplier has its own input buffer, the use of a buffer operational amplifier reduces the error of the cosine block functioning in feedback, and thus decreases the need to adjust the trim resistors. R_{16} restricts the saturation current of limiting diodes $D_3 - D_6$.

The 8th order approximation circuit successfully implements 3 periods of cosine-like even periodic function through the cascaded stages of multiplication and addition. The variable resistors enable precise adjustment of

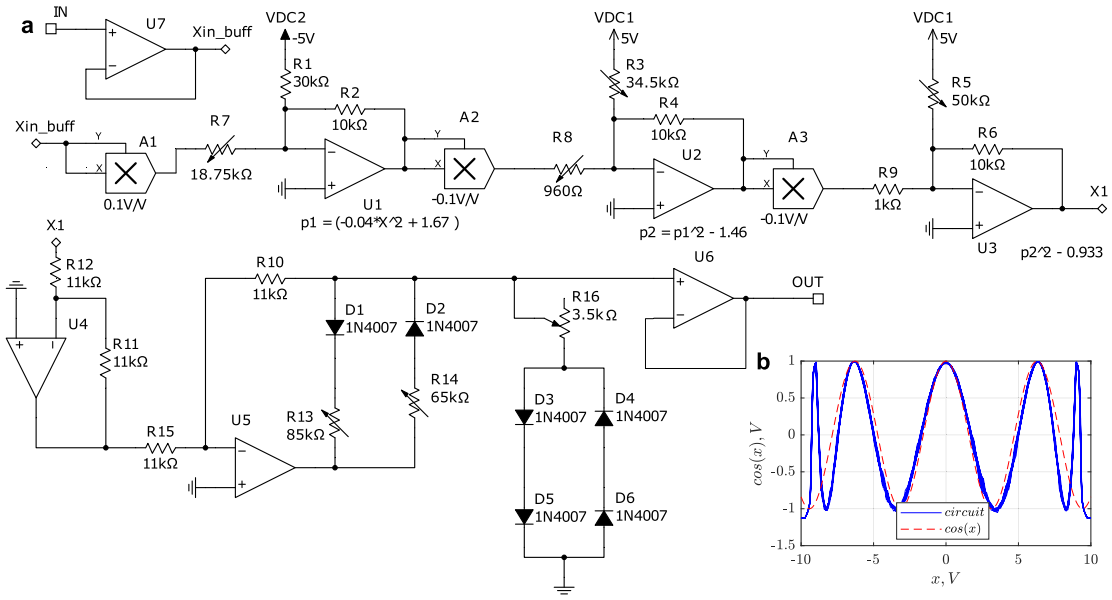

Figure 15. (a) Electronic schematic diagram of the cosine approximation block and (b) its transfer characteristics. Components used include analog multipliers (AD633JN), operational amplifiers (MC33078, OPA2134), and diodes (1N4007).

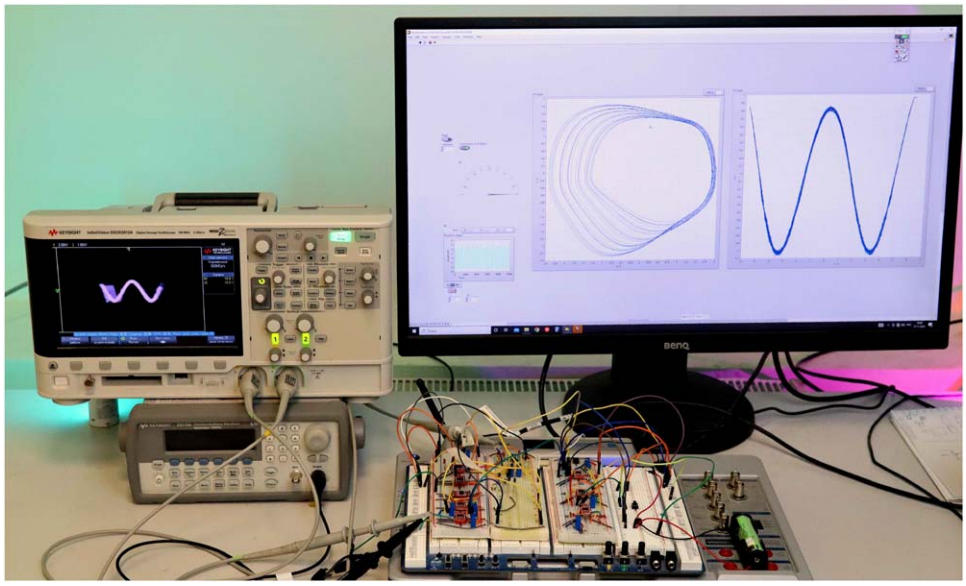

Figure 16. Photograph of the experimental bench.

the transfer characteristic, compensating for component non-idealities and optimizing the dynamical behavior. The final output stage through U_6 provides the complete cosine approximation with the desired characteristics for chaotic attractor implementation.

6.3. Circuit implementation under polynomial approximation

The circuit experimental setup is depicted in figure 16. A 16-bit ADC (Analog-to-Digital Converter) is employed to acquire data from the circuit, while an oscilloscope provides real-time visualization of the cosine function approximation. To validate the system, we compare results across four implementation levels, as shown in figure 17: (a) the direct numerical solution of equation (19) using the 4th-order Runge-Kutta method, (b) SPICE-based simulation incorporating an ideal mathematical cosine function, (c) SPICE-based simulation using an approximated cosine function (as outlined in figure 15), and (d) the physical circuit output with the approximated cosine function.

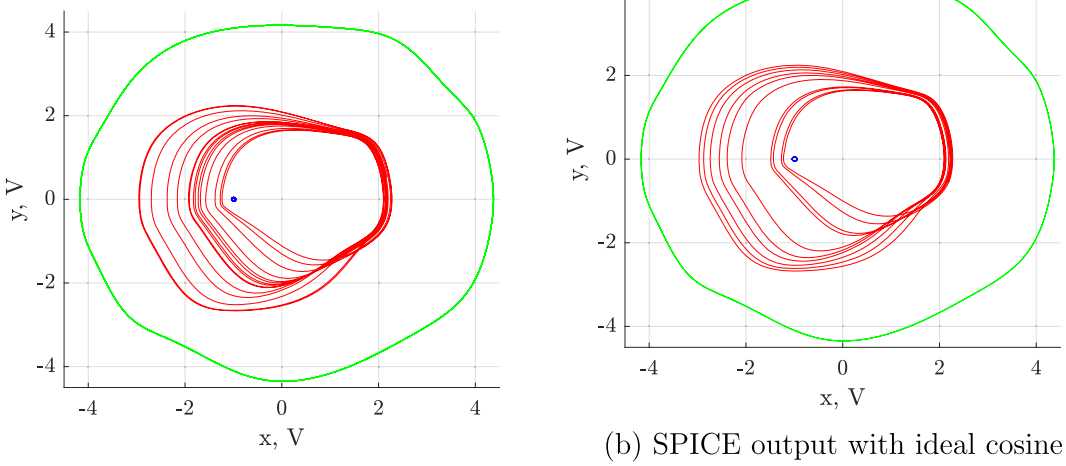

(a) Coexisting attractors for system (19)

(b) SPICE output with ideal cosine function for system (20)

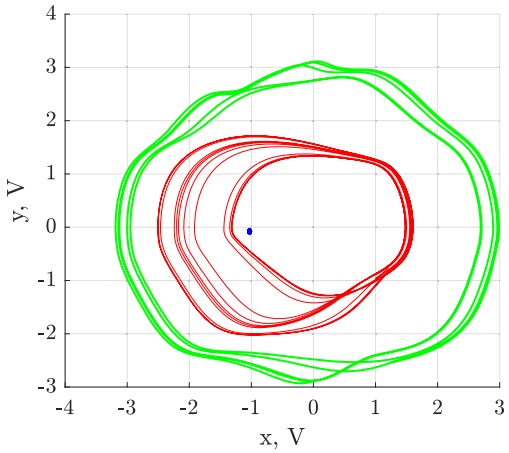

(c) SPICE output with approximated cosine function for system (20)

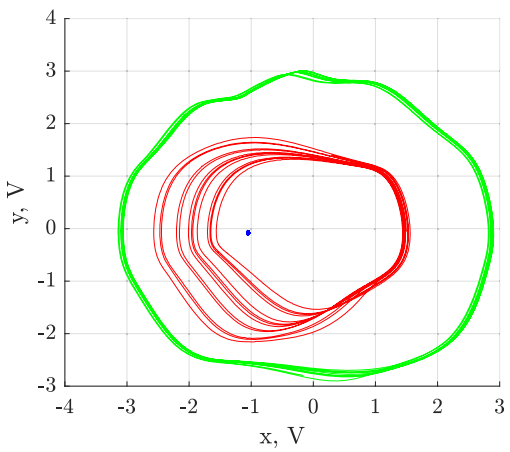

(d) Real circuit output with approximated cosine function for system (20)

Figure 17. Comparison of coexisting attractors across different implementation levels: mathematical model, SPICE simulations (with ideal and approximated cosine functions), and physical circuit realization. Initial data: $(x(0), y(0), z(0)) = (0,0.2,0)$ (blue), $(0, 2, 0)$ (red), $(0, 3, 0)$ (green).

The results demonstrate the existence of coexisting attractors across all cases, confirmed using three sets of initial conditions: $(x(0), y(0), z(0)) = (0, 0.2, 0)$ (blue), $(0, 2, 0)$ (red), and $(0, 3, 0)$ (green). The numerical solution and SPICE simulation with the ideal cosine function exhibit a high degree of accuracy and consistency. Meanwhile, the SPICE simulation with the approximated cosine function captures additional nonlinear effects, resulting in dynamics closely aligned with the physical circuit's behavior.

The match between the analog circuit and the mathematical model has limited accuracy, which is typical in the comparison of nonlinear electric or mechanical systems and computer simulations [61, 62]. The presented experiment confirms the correctness of the system circuit implementation, and, more generally, the possibility of the existence of multiple attractors in real physical system, as well as the possibility to switch them by changing initial conditions.

7. Conclusions

This paper presented a three-dimensional chameleon system derived from the classical Duffing oscillator. By transforming an externally driven Duffing system into an internally modulated autonomous system, we demonstrated that coupling the driving force with the system's state can generate complex dynamical behaviors.

Through rigorous mathematical analysis, we established some basic properties of the system, including its dissipativity, local stability, and the occurrence of a supercritical Hopf bifurcation at $c = 0$. We demonstrated that $c = 0$ serves as a critical boundary distinguishing hidden chaotic regimes from self-excited chaotic

dynamics. Using a continuation diagram, we observed the system's transition from a stable equilibrium to periodic orbits and eventually to self-excited chaos through a supercritical Hopf bifurcation and a period-doubling cascade.

The study emphasized the simplified case ($c = 0$) with multistable dynamics. We observed the coexistence of four nested hidden chaotic attractors, with chaotic intensity monotonically decreasing as the distance from the equilibrium increased. Bifurcation diagrams revealed the effects of the varying parameters b and ω. The introduction of an offset boosting mechanism demonstrated the ability to control attractor positions.

To validate the theoretical findings, we designed and implemented an electronic circuit that physically realizes a typical system with a point attractor, a hidden chaotic attractor, and a period-1 attractor. The circuit employed an 8th-order polynomial approximation of the cosine function. The experimental result aligned with SPICE simulation, confirming the model's robustness.

This work advances our understanding of chameleon chaotic systems. The synthesis of theoretical analysis, numerical simulation, and experimental validation presented here facilitates the study and application of chameleon systems with rich multistable dynamics. Future research may explore extensions to higher-dimensional systems and develop control strategies for real-world implementations.

Acknowledgments

Bo Sang was supported by the Shandong Provincial Natural Science Foundation (No. ZR2018MA025), Timur Karimov was supported by the Russian Science Foundation (RSF), Project No. 23-79-10151.

Data availability statement

All data that support the findings of this study are included within the article (and any supplementary files).

ORCID iDs

Bo Sang https://orcid.org/0000-0003-3978-2225
Irfan Ahmad https://orcid.org/0000-0002-7156-9056
Timur Karimov https://orcid.org/0000-0002-9860-8211
Vyacheslav Rybin https://orcid.org/0000-0002-6515-0224
Denis Butusov https://orcid.org/0000-0002-8941-4220
Ning Wang https://orcid.org/0000-0002-4453-8588

References

[1] Meyers R A 2002 *Encyclopedia of Physical Science and Technology* vol 6 (Elsevier)
[2] Alexeeva T A, Kuznetsov N V and Mokaev T N 2021 Study of irregular dynamics in an economic model: attractor localization and Lyapunov exponents *Chaos Solitons Fractals* **152** 111365
[3] Vaidyanathan S *et al* 2023 A novel 3-D jerk system, its bifurcation analysis, electronic circuit design and a cryptographic application *Electronics* **12** 2818
[4] Nwachioma C and Pérez-Cruz J H 2021 Analysis of a new chaotic system, electronic realization and use in navigation of differential drive mobile robot *Chaos Solitons Fractals* **144** 110684
[5] Hannachi F 2019 Analysis, dynamics and adaptive control synchronization of a novel chaotic 3-D system *SN Applied Sciences* **1** 158
[6] Annaswamy A M 2023 Adaptive control and intersections with reinforcement learning *Annu. Rev. Control Robot. Auton. Syst.* **6** 65–93
[7] Li C, Hu W, Sprott J C and Wang X 2015 Multistability in symmetric chaotic systems *Eur. Phys. J. Spec. Top.* **224** 1493–506
[8] Leonov G A and Kuznetsov N V 2013 Hidden attractors in dynamical systems. From hidden oscillations in Hilbert-Kolmogorov, Aizerman, and Kalman problems to hidden chaotic attractor in Chua circuits *Int. J. Bifurcation and Chaos* **23** 1330002
[9] Stankevich N V, Kuznetsov N V, Leonov G A and Chua L O 2017 Scenario of the birth of hidden attractors in the Chua circuit *Int. J. Bifurcation and Chaos* **27** 1730038
[10] Kuznetsov N V, Mokaev T, Ponomarenko V, Seleznev E, Stankevich N V and Chua L O 2023 Hidden attractors in Chua circuit: mathematical theory meets physical experiments *Nonlinear Dyn.* **111** 5859–87
[11] Kuznetsov N V, Leonov G A and Vagaitsev V I 2010 Analytical-numerical method for attractor localization of generalized Chua's system *IFAC Proc.* **43** 29–33
[12] Leonov G A, Kuznetsov N V and Vagaitsev V I 2011 Localization of hidden Chua's attractors *Phys. Lett.* A **375** 2230–3
[13] Wu Q, Hong Q, Liu X, Wang X and Zeng Z 2020 A novel amplitude control method for constructing nested hidden multi-butterfly and multiscroll chaotic attractors *Chaos Solitons Fractals* **134** 109727
[14] Tian H, Wang Z, Zhang P, Chen M and Wang Y 2021 Dynamic analysis and robust control of a chaotic system with hidden attractor *Complexity* **2021** 8865522
[15] Zhou T and Chen G 2006 Classification of chaos in 3-D autonomous quadratic systems-I: basic framework and methods *Int. J. Bifurcation and Chaos* **16** 2459–79
[16] Wei Z, Sprott J C and Chen H 2015 Elementary quadratic chaotic flows with a single non-hyperbolic equilibrium *Phys. Lett.* A **379** 2184–7

[17] Rajagopal K, Pham V T, Tahir F R, Akgul A, Abdolmohammadi H R and Jafari S 2018 Dynamics, circuit implementation, and communication application of a chaotic jerk system with non-hyperbolic equilibrium *Pramana* **90** 1–9
[18] Cai X, Liu L, Wang Y and Liu C 2021 A 3D chaotic system with piece-wise lines shape non-hyperbolic equilibria and its predefined-time control *Chaos Solitons Fractals* **146** 110904
[19] Li C and Hai W 2018 Constructing multiwing attractors from a robust chaotic system with non-hyperbolic equilibrium points *Automatika* **59** 184–93
[20] Li C and Sprott J C 2014 Chaotic flows with a single nonquadratic term *Phys. Lett.* A **378** 178–83
[21] Jafari S, Sprott J C and Nazarimehr F J 2015 Recent new examples of hidden attractors *Eur. Phys. J. Spec. Top.* **224** 1469–76
[22] Wang X and Chen G 2012 A chaotic system with only one stable equilibrium *Commun. Nonlinear Sci. Numer. Simul.* **17** 1264–72
[23] Wang X, Akgul A, Cicek S, Pham V T and Hoang D V 2017 A chaotic system with two stable equilibrium points: dynamics, circuit realization and communication application *Int. J. Bifurcation and Chaos* **27** 1750130
[24] Rech P C 2022 Self-excited and hidden attractors in a multistable jerk system *Chaos Solitons Fractals* **164** 112614
[25] Pham V T, Jafari S, Volos C and Kapitaniak T 2016 A gallery of chaotic systems with an infinite number of equilibrium points *Chaos Solitons Fractals* **93** 58–63
[26] Molaie M, Jafari S, Sprott J C and Golpayegani S M 2013 Simple chaotic flows with one stable equilibrium *Int. J. Bifurcation and Chaos* **23** 1350188
[27] Jafari S and Sprott J C 2013 Simple chaotic flows with a line equilibrium *Chaos Solitons Fractals* **57** 79–84
[28] Kumarasamy S, Banerjee M, Varshney V, Shrimali M D, Kuznetsov N V and Prasad A 2023 Saddle-node bifurcation of periodic orbit route to hidden attractors *Phys. Rev.* E **107** L052201
[29] Leutcho G D and Kengne J 2018 A unique chaotic snap system with a smoothly adjustable symmetry and nonlinearity: chaos, offset-boosting, antimonotonicity, and coexisting multiple attractors *Chaos Solitons Fractals* **113** 275–93
[30] Li B, Sang B, Liu M, Hu X, Zhang X and Wang N 2023 Some jerk systems with hidden chaotic dynamics *Int. J. Bifurcation and Chaos* **33** 2350069
[31] Dong C, Yang M, Jia L and Li Z 2024 Dynamics investigation and chaos-based application of a novel no-equilibrium system with coexisting hidden attractors *Physica* A **633** 129391
[32] Jafari M A, Mliki E, Akgul A, Pham V T, Kingni S T, Wang X and Jafari S 2017 Chameleon: the most hidden chaotic flow *Nonlinear Dyn.* **88** 2303–17
[33] Natiq H, Said M R, Ariffin M R, He S, Rondoni L and Banerjee S 2018 Self-excited and hidden attractors in a novel chaotic system with complicated multistability *Eur. Phys. J. Plus* **133** 557
[34] Signing V F, Tegue G G, Kountchou M, Njitacke Z T, Tsafack N, Nkapkop J D, Etoundi C L and Kengne J 2022 A cryptosystem based on a chameleon chaotic system and dynamic DNA coding *Chaos Solitons Fractals* **155** 111777
[35] Tiwari A, Nathasarma R and Roy B K 2024 A new time-reversible 3D chaotic system with coexisting dissipative and conservative behaviors and its active non-linear control *J. Franklin Inst.* **361** 106637
[36] Leutcho G D, Kengne J, Kengne L K, Akgul A, Pham V T and Jafari S 2020 A novel chaotic hyperjerk circuit with bubbles of bifurcation: mixed-mode bursting oscillations, multistability, and circuit realization *Phys. Scr.* **95** 075216
[37] Jafari S, Rajagopal K, Hayat T, Alsaedi A and Pham V T 2019 Simplest megastable chaotic oscillator *Int. J. Bifurcation and Chaos* **29** 1950187
[38] Vijayakumar M D, Natiq H, Meli M I T, Leutcho G D and Njitacke Z T 2022 Hamiltonian energy computation of a novel memristive mega-stable oscillator (MMO) with dissipative, conservative and repelled dynamics *ChaosSolitons Fractals* **155** 111765
[39] Bao B C, Bao H, Wang N, Chen M and Xu Q 2017 Hidden extreme multistability in memristive hyperchaotic system *Chaos Solitons Fractals* **94** 102–11
[40] Leutcho G D, Woodward L and Blanchard F 2023 Nonlinear dynamics of a single-gap terahertz split-ring resonator under electromagnetic radiation *Chaos* **33** 103131
[41] Sambas A *et al* 2022 A novel 3D chaotic system with line equilibrium: multistability, integral sliding mode control, electronic circuit, FPGA implementation and its image encryption *IEEE Access* **10** 68057–74
[42] Vijayakumar M D, Natiq H, Leutcho G D, Rajagopal K, Jafari S and Hussain I 2022 Hidden and self-excited collective dynamics of a new multistable hyper-jerk system with unique equilibrium *Int. J. Bifurcation and Chaos* **32** 2250063
[43] Vaidyanathan S, Azar A T, Hameed I A, Benkouider K, Tlelo-Cuautle E, Ovilla-Martinez B, Lien C H and Sambas A 2023 Bifurcation analysis, synchronization and FPGA implementation of a new 3-D jerk system with a stable equilibrium *Mathematics* **11** 2623
[44] Benkouider K, Sambas A, Bonny T, Al Nassan W, Moghrabi I A R, Sulaiman I M, Hassan B A and Mamat M 2024 A comprehensive study of the novel 4D hyperchaotic system with self-exited multistability and application in the voice encryption *Sci. Rep.* **14** 12993
[45] Sambas A, Miroslav M, Vaidyanathan S, Ovilla-Martínez B, Tlelo-Cuautle E, El-Latif A A, Abd-El-Atty B, Benkouider K and Bonny T 2024 A new hyperjerk system with a half line equilibrium: multistability, period doubling reversals, antimonotonocity, electronic circuit, FPGA design, and an application to image encryption *IEEE Access* **12** 9177–94
[46] Zhou R, Gu Y, Cui J, Ren G and Yu S 2021 Nonlinear dynamic analysis of supercritical and subcritical Hopf bifurcations in gas foil bearing-rotor systems *Nonlinear Dyn.* **103** 2241–56
[47] Zhao H, Lin Y and Dai Y 2017 Hopf bifurcation and hidden attractor of a modified Chua's equation *Nonlinear Dyn.* **90** 2013–21
[48] Liu M, Sang B, Wang N and Ahmad I 2021 Chaotic dynamics by some quadratic jerk systems *Axioms* **10** 227
[49] Li C, Akgul A, Bi L, Xu Y and Zhang C 2024 A chaotic jerk oscillator with interlocked offset boosting *Eur. Phys. J. Plus* **139** 1–10
[50] Li C, Wang X and Chen G 2017 Diagnosing multistability by offset boosting *Nonlinear Dyn.* **90** 1335–41
[51] Gao X 2024 Hamilton energy of a complex chaotic system and offset boosting *Phys. Scr.* **99** 015244
[52] Zhang X, Li C, Lei T, Fu H and Liu Z 2024 Offset boosting in a memristive hyperchaotic system *Phys. Scr.* **99** 015247
[53] Yang Y, Huang L, Xiang J and Guo Q 2021 Three-dimensional sine chaotic system with multistability and multi-scroll attractor *IEEE Trans. Circuits Syst. II Express Briefs* **69** 1792–6
[54] Ramar R 2023 Design of a new chaotic system with sine function: dynamic analysis and offset boosting control *Chaos Th. Appl.* **5** 118–26
[55] Zhang C, Zhang B, Chen J, Pan A, Tan Z, Yao Y, Gui R and Cheng G 2024 Controllable multi-scroll with multi-wing, grid-scroll, and multi-directional grid-scroll chaotic attractors in a chaotic system with implicit Duffing equation *Eur. Phys. J. Plus* **139** 492
[56] Vincent T L, Mees A I and Jennings L S 1990 *Dynamics of complex interconnected biological systems Mathematical Modelling Vol. 6* (Birkhäuser) (https://doi.org/10.1007/978-1-4684-6784-0)
[57] Jia Y 2020 Review of nonlinear vibration energy harvesting: Duffing, bistability, parametric, stochastic and others *J. Intell. Mater. Syst. Struct.* **31** 921–44

[58] Kovacic I and Brennan M J 2011 *The Duffing equation: Nonlinear Oscillators and Their Behaviour* (Wiley) (https://doi.org/10.1002/9780470977859)
[59] Vialar T 2009 *Complex and Chaotic Nonlinear Dynamics Advances in Economics and Finance, Mathematics and Statistics* (Springer) (https://doi.org/10.1007/978-3-540-85978-9)
[60] Dang-Vu H and Delcarte C 2000 *Bifurcations et Chaos (Ellipses)*
[61] Karimov A, Rybin V, Kopets E, Karimov T, Nepomuceno E and Butusov D 2023 Identifying empirical equations of chaotic circuit from data *Nonlinear Dyn.* **111** 871–86
[62] Karimov A, Rybin V, Dautov A, Karimov T, Bobrova Y and Butusov D 2023 Mechanical chaotic Duffing system with magnetic springs *Inventions* **8** 19